# Numerical Investigation of Influence of Eccentricity on the Hydrodynamics of a Ship Maneuvering into a Lock

# Qingjie Meng<sup>1,2</sup>, Decheng Wan<sup>1,2</sup>\* and Wenhua Huang<sup>3</sup>

State Key Laboratory of Ocean Engineering, School of Naval Architecture, Ocean and Civil Engineering, Shanghai Jiao Tong University,
 Collaborative Innovation Center for Advanced Ship and Deep-Sea Exploration, Shanghai 200240, China
 School of Science, Huzhou University, Huzhou 313000, China
 \*Corresponding author: dcwan@sjtu.edu.cn

#### **Abstract**

By solving the unsteady RANS (Reynolds Averaged Navier–Stokes) equations in combination with the k- $\omega$  SST turbulence model, the unsteady viscous flow around a 12000TEU ship model while entering the Third Set of Panama Locks with different ecentricity is simulated and the hydrodynamic forces, vertical displacement are predicted and analyzed. Overset grid technology is used to maintain grid orthogonality. The effects of the free surface are taken into account. A benchmark test case is designed first to validate the capability of the present methods in the prediction of the viscous flow around the ship when maneuvering into the lock. The accumulation of water in front of the ship during entry into a lock is noticed, which causes the increase of the velocity of the return flow. A set of systematic computations with different ecentricity are then carried out to examine the effect of ecentricity on the ship-lock hydrodynamic interaction while entering the lock. With higher ecentricity, higher hydrodynamic forces and higher yawing moment is observed, which cause greater risk of contact of a ship with the lock infrastructure.

**Keywords:** lock; 12000TEU, overset grid; ship-lock hydrodynamic interaction; ecentricity

### Introduction

The lock approach will always be accompanied with bank effect on the hydrodynamic forces, since ships can have very small side margins in the lock. Besides, ships are also allowed with a very small under keel clearance to exploit the lock maximally and thus typically a high blockage. The high blockage influences the flow along the ship hull, increasing the relative speed between the ship and inverse flow. Furthermore, the high blockage also causes a so called piston effect, which provokes an accumulation of water during ship's entry into the lock. The frictional resistance increases and water piles up inside the lock resulting in higher resistance. What's more, it is very difficult to keep the ship maneuvering along the lock's centerline. This obviously produces a worse situation for a ship approaching a lock. Overall, a ship will experience a particular hydrodynamic force caused by the hydrodynamic interaction with the lock, during the entering manoeuvre into a lock. This hydrodynamic interaction has a significant influence on the ship navigation safety. The investigation on the effects of eccentricity is of crucial importance for safe operation and effective control of ships passing through a lock.

Several methods have been used to examine the feasibility to use locks for large vessels. Although real scale and model scale tests can be carried out, reliable simulations are necessary to examine infrastructure in an affordable and efficient manner. Vrijburcht (1988) used six-waves-model to calculate the translation waves generated by the lock entry. Vergote (2012) improved the six-waves-model model. Chen (2010) developed a viscous frictional model to calculate dynamical ship-lock interaction problem. Delefortrie et al. (2008, 2009) analyzed the navigation behavior of different ship models in the Third Set of Panama Locks and the influences of approach wall configurations, eccentricities, propeller rates, approaching scenarios and under keel clearances were also discussed. Verwilligen and Richter (2012) investigated the entering manoeuvre of full form ships into the Terneuzen West Lock by means of model testing, full scale trials and real-time simulations. Wang et al. (2014) studied the viscous flow around a ship when entering the Pierre Vandamme Lock based on the CFD package Fluent, but the free surface was neglected.

The objective of this study is to examine the effects of eccentricity on a 12000TEU ship model when entering the Third Set of Panama Locks by predict and analyze the viscous flow and hydrodynamic forces of the ship model maneuvering into the lock with different lateral position. At

first, the capability of the present method for the prediction of the viscous flow around the ship model is validated by the good agreement of the predicted results with the corresponding experimental data. Then a series of systematic computations with different lateral position are carried out and the predicted forces and moments, vertical displacement are analyzed to investigate the viscous flow around the ship and the influence of the eccentricity on the ship-lock hydrodynamic interaction during its entry into a lock.

The computation is carried out by an in-house CFD code based on the Finite Difference Method (FDM). The code was proved to be competent in simulating the unsteady viscous flow around a ship in confined water (Meng et al. 2014). Finite Difference Method (FDM) can be used even when high cell aspect ratio is present and thus is very suitable to solve low speed problems. Refinement grid are used only in the vertical direction to ensure the grid number within an acceptable range as well as the accuracy of the capture of the free surface. When a ship entering into a lock, a mass of water will be pushed into the lock, which might causes the initial bow up and a significantly increased resistance. So, to make our prediction more reasonable, the effects of the free surface is taken into account. Besides, the overset grid technique is introduced to avoid the deterioration of the computational accuracy caused by the mesh distortion near the boundary layer region when the ship moves with large amplitude.

#### **Mathematical Method**

# Governing Equations

The viscous flow around the ship is assumed incompressible and the numerical problem is described by RANS equations coupled with the time-averaged continuity equation in non-dimensional tensor form:

$$\frac{\partial U_i}{\partial t} + U_j \frac{\partial U_i}{\partial x_j} = -\frac{\partial \hat{p}}{\partial x_i} + \frac{\partial}{\partial x_j} \left[ Re_{\text{eff}}^{-1} \left( \frac{\partial u_i}{\partial x_j} + \frac{\partial u_j}{\partial x_i} \right) \right] + S_i$$
 (1)

$$\frac{\partial U_i}{\partial x_i} = 0 \tag{2}$$

where  $U_i = (\mathbf{u}, \mathbf{v}, w)$  denote the Reynolds-average velocity components;  $\mathbf{x}_i = (\mathbf{x}, \mathbf{y}, \mathbf{z})$  represent the independent coordinate directions;  $S_i$  stand for a body force due, for instance, to a propeller model, respectively; the piezometric pressure  $\hat{p}$  and the effective Reynolds number  $Re_{eff}$  are:

$$\hat{p} = p_{abs} / \rho U_0^2 + z / Fr^2 + 2k/3$$
 (3)

$$Re_{\rm eff}^{-1} = 1/Re + \gamma_{\rm c} \tag{4}$$

with k the turbulence kinetic energy,  $p_{abs}$  the absolute pressure, z the local vertical elevation and  $\gamma$ , the non-dimensional turbulent viscosity obtained from a turbulence model. All the variables and properties are nondimensionalized by the reference velocity U, ship length  $L_{pp}$  and the mass density of the water  $\rho$ .

#### Turbulence Model

The k- $\omega$  SST turbulence model was chosen to close the RANS equations. As the k- $\omega$  SST turbulence model employs the k- $\omega$  model near walls and the k- $\varepsilon$  model away from walls, it gives highly accurate predictions of the onset and the amount of flow separation under adverse pressure gradients.

The turbulence kinetic energy k is computed using a blended k- $\varepsilon/k$ - $\omega$  model (Menter, F. R. 1994). In this model, the eddy viscosity  $v_{\epsilon}$ , turbulence kinetic energy k and the turbulence specific dissipation rate  $\omega$  can be computed from:

$$v_t = \frac{k}{\omega} \tag{5}$$

$$\frac{\partial k}{\partial t} + \left( U_j - \sigma_k \frac{\partial V_t}{\partial x_i} \right) \frac{\partial k}{\partial x_i} - \frac{1}{R_k} \nabla^2 k + s_k = 0$$
 (6)

$$\frac{\partial \omega}{\partial t} + \left( U_j - \sigma_\omega \frac{\partial V_t}{\partial x_j} \right) \frac{\partial \omega}{\partial x_j} - \frac{1}{R_w} \nabla^2 \omega + s_\omega = 0 \tag{7}$$

where the source terms, effective Reynolds numbers, and turbulence production can be described as:

$$S_k = R_k \left( -G + \beta^* \omega k \right) \tag{8}$$

$$S_{\omega} = R_{\omega} \left( -\gamma \frac{\omega}{k} G + \beta \omega^{2} + 2(I - F_{l}) \sigma_{\omega^{2}} \frac{I}{\omega} \frac{\partial k}{\partial x_{i}} \frac{\partial \omega}{\partial x_{i}} \right)$$

$$(9)$$

$$R_{k/\omega} = \frac{1}{1/Re + \sigma_{k/\omega} V_{t}} \tag{10}$$

$$G = \tau_{ij} \frac{\partial u_i}{\partial u_i} = v_i \left[ \left( u_y + v_x \right)^2 + \left( u_z + w_x \right)^2 + \left( v_z + w_y \right)^2 + 2u_x^2 + 2v_y^2 + 2w_z^2 \right]$$
(11)

with  $\beta$ ,  $\beta^*$ ,  $\sigma_k$ ,  $\sigma_\omega$  constants and  $F_I$  the blending function, which is designed to be one in the sublayer and logarithmic regions of boundary layers and gradually switches to zero in the wake region to take advantage of the strengths of the k- $\omega$  and k- $\varepsilon$  models in different position. The model constants are calculated locally as a weighted average, i.e.,  $\phi = F_1 \phi_1 + (1 - F_1) \phi_2$  where  $\phi_1$  denote the standard k- $\omega$  and  $\phi_2$  represent k- $\varepsilon$  values.

### Free Surface

We capture the location of the transient free surface using level set function  $\phi$  (Osher, S., & Sethian, J. A., 1988; Sussman et al. 1994; Sethian and Smereka. 2003), whose value is related to the distance to the interface. And the value of  $\phi$  is arbitrarily set to positive in water and negative in air and the iso-surface  $\phi$ =0 represents the free surface. Since the free surface is considered a material interface, then it should satisfy the kinematic free surface boundary condition and can be described as:

$$\frac{\partial \phi}{\partial t} + \mathbf{v} \cdot \nabla \phi = 0 \tag{12}$$

The following conditions for the velocity and pressure should be satisfied:

$$\nabla \mathbf{v} \cdot \mathbf{n} = 0 \tag{13}$$

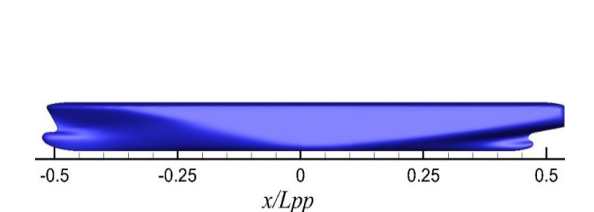
$$\hat{p} = \frac{z}{Fr^2} \tag{14}$$

where  $n = -\frac{\nabla \phi}{|\nabla \phi|}$  is the unit normal vector to the free surface, pointing from water to air.

To make sure that the level set function is kept a distance function after the transport step, a reinitialization procedure is used in which the points close to the free surface are reinitialized geometrically, while a transport equation is solved for all other points.

# **Simulation Design**

The problem under study is a 12000TEU container carrier moving into the Third Set of Panama Lock with different eccentricity. The ship is a 1/80 scale model of 12000TEU. The geometry of the ship model is shown in Fig. 1. A 1/80 scale model of a lock and approach channel is designed according to the preliminary design of the Panama Canal Third Set of Locks. The geometry and the principal dimensions of the lock model is shown in Fig. 2. These geometry is a benchmark on the ship behavior in locks, tested in Flanders Hydraulics Research in 2007-2008. Numerical results are compared with the experimental data by Vantorre, M. et al. (2012).



O. 1581.pp 1.521.pp 1.331.pp Open water

Fig.1 Geometry of the 12000TEU hull

Fig.2 Geometry of the lock

All the present work is conducted on a computer cluster which consists of 16 Intel Xeon E5520 (2.27GHz) processors, with 8 cores and 24GB RAM per processor. Each computation is performed using 16 cores and costs about 144 hours of wall clock time.

#### Case Conditions

The ship model is Lpp=4.35 m long with 0.19 m draft. Table 1 gives the principal dimensions of the ship model. Three cases are studied numerically. Case A, with lateral position  $\Delta y = 0.0$  mm, is designed according to the benchmark test and selected for validation. Numerical tests cases A1 and A2 are also carried out to study the effects of eccentricity on the hydrodynamic forces acting on the ship, with lateral positions:  $\Delta y = 7.5$  mm and  $\Delta y = 19$  mm model scale, respectively. Details of the case conditions are shown in table 2. Free surface is considered for all cases.

Item	Symbol	Unit	Value
Length between perpendiculars	$L_{pp}$	m	4.350
Breadth (molded)	B	m	0.613
Draft (molded)	D	m	0.190
Blockage coefficient	$C_{\scriptscriptstyle B}$		0.65

Table 1 Principal dimensions of the 12000TEU model

Table 2 Details of the case conditions

Conditions			Test No.		
			A	A1	A2
water depth	h	m	0.228	0.228	0.228
Froude number	Fr	-	0.0176	0.0176	0.0176
Reynolds number	Re	$\times 10^{\circ}$	4.392	4.392	4.392
Depth/draft ratio	h/D	-	1.2	1.2	1.2
lateral position	$\Delta y$	mm	0.0	7.5	19

Computational Domain, Coordinate System and Boundary Conditions

The computational domain, which extend within  $-1.62 \le x \le 5.10$ ,  $-0.0524 \le z \le 0.17$ ,  $-0.079 \le y \le 0.079$  for the lock and  $-0.313 \le y \le 0.313$  for the approach channel, covers the whole ship

considering the asymmetry of the flow field. A right-handed Cartesian coordinate system is located at the door of the lock. The longitudinal Ox-axis points to the approach channel, the Oz-axis is vertical and points upward, and the undisturbed free surface is taken as the plane z=0. The origin of the coordinates is located at the intersection of the waterline, the center plane of the lock and the plane of the lock door. A schematic diagram indicating the coordinate system and the computational domain is given in Fig. 3. The boundary conditions mimic the conditions in the FHR (Flanders Hydraulics Research) towing tank for later comparison of the numerical results with the experimental data. The computational domain is made up of three kinds of boundaries: no-slip wall (hull surface), far-field (z=zmax) and slip wall (all other boundaries).

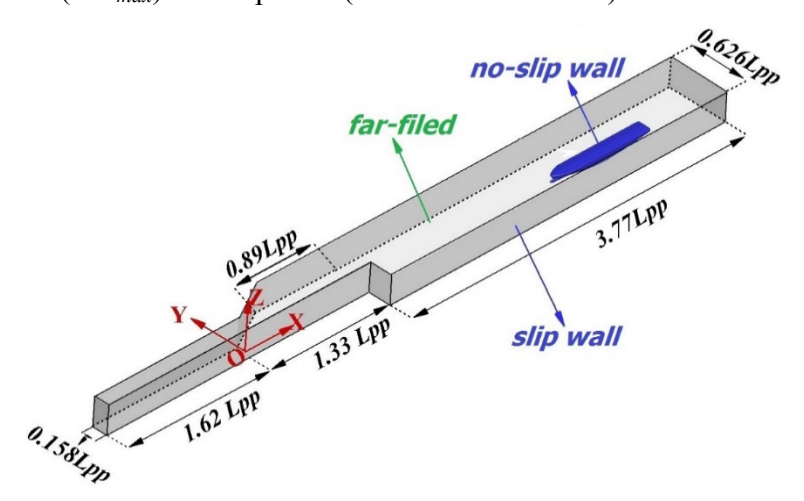


Fig.3 Computational domain, coordinate system and boundary conditions

# Grid Design

For all cases, structured grids are used and overset gird technique is utilized to keep the orthogonality of the grid under the consideration of keeping a good computational accuracy.

A sketch of the grid distribution is shown in Figs. 4-5, where the grids are coarsened for clarity. The grid consists of a background orthogonal grid, which mimics the towing tank, and a boundary layer curvilinear grid which conforms to the ship geometry where two clusters of grid points are concentrated around the bow and stern regions. The boundary layer grid is generated with a grid spacing at the hull satisfying the condition y+<1 for all case. All the grids are refined in the vertical direction in  $-0.003 \le z \le 0.003$ , where the free surface is expected.

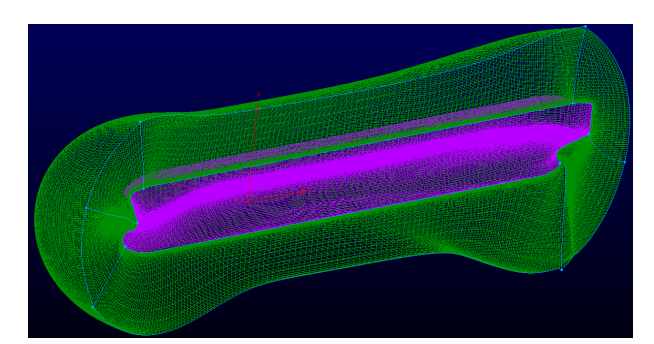


Fig.4 boundary layer curvilinear grid of the ship model

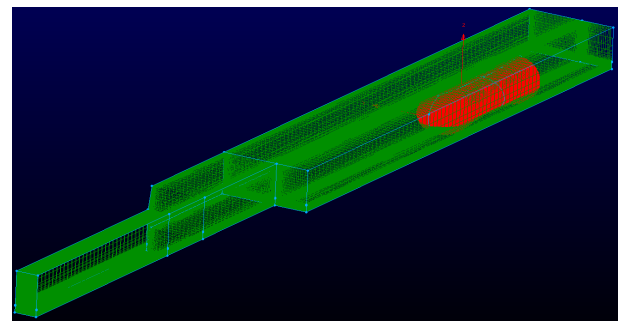


Fig.5 a sketch of the grid distribution

#### **Results of Benchmark Test Case**

Test case A, designed according to the experiment, is used to confirm the capability of present method in the prediction of the viscous flow around the ship model while maneuvering into the lock.

Comparisons between computed and experimental data is presented for the x-direction hydrodynamic force X, y-direction hydrodynamic force Y, the moment around the z-axis N and the vertical displacement of the fore and aft perpendiculars zFP and zAP.

For a clear insight of the viscous flow around the ship during the maneuvering into the lock, three special instants, shown in Fig. 6, are defined. At time T1, the ship is still moving in the approach channel, while forebody of the ship has entered the lock at time T2. At time T3, the ship has entered the lock.



Fig. 6 Definition of three certain times

Fig. 7 Coordinate systems for hydrodynamic forces and moment

#### Hydrodynamic Forces

Coordinate systems for hydrodynamic forces and moment is shown in Fig. 7. Fig. 8 presents the comparison of the computed results and experimental data for the time history of hydrodynamic forces and moment, where the x axis represents the position of the bow. Notice that the x coordinate values change from 2.5 to -1 when the ship maneuvering from the approach channel into the lock, as the coordinate system, shown in Fig. 3, is located at the door of the lock and the longitudinal Oxaxis is pointing to the approach channel. The predicted results show good agreement with measured data and exhibits consistent oscillation compared with the experimental data.

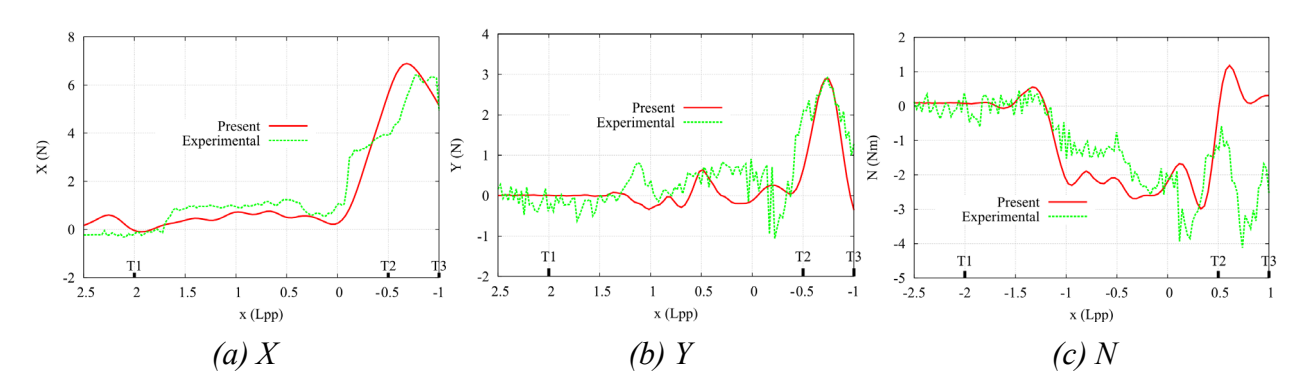


Fig. 8 Time history of the hydrodynamic forces and moment

Taking longitudinal force X as an example, during maneuverer the ship into the lock, it goes through three stages. In the first stage, the hydrodynamic force X is very small with insignificant oscillation when the ship maneuvers in the approach channel. This is caused by the extremely low ship speed. Then, a soaring increase of the hydrodynamic force X is noticed during the ship maneuvering into the lock. During the entry into the lock, an accumulation of water is provoked in front of the ship because of the piston effect. This induces the increase of the bow pressure and the decrease of the stern pressure, which causes a dramatically increase of the viscous pressure resistance. Also, an increased friction resistance will occur because of the higher velocities of the return flow. Accordingly, the longitudinal force X increases. At the least stage, once the ship has entered the lock, a significant decrease of the resistance force can be noticed. When the ship has entered the lock, water is evacuated out of the lock. As a result, the pressure difference between the fore and aft part of the ship decreases, reducing the oscillations. The hydrodynamic force Y and the moment Y also shows the same tendency. Bank effect develops in case of an eccentric approach until the ship has entered the lock. The asymmetric flow around the ship induced by the vicinity of

banks causes pressure differences between port and starboard sides. The velocity will increase alongside the nearest bank, causing a pressure decrease. As a result, a lateral force will act on the ship, directed towards the closest bank, as well as a yawing moment pushing the ship bow towards the center of the waterway. Once the ship has entered the lock, the asymmetric flow disappears and the lateral force, as well as the yawing moment falls to zero. This is confirmed by the results shown in Figs. 8b and 8c.

# Vertical Displacements

Piston effect, which provokes an accumulation of water during entry into a lock, causes the increase of the return flow velocity and a sinkage of the water level in the vicinity of the ship, which induces a general sinkage of the ship. The return flow of the ship causes a pressure drop around the ship, according to the Bernoulli principle. As a result, the ship also moves vertically downward. Generally, the pressure drop will not be distributed equally over the ship, causing a trim.

The mean sinkage  $\sigma$  and trim  $\tau$  were determined from the calculated sinkage force Z and trim moment M using the formulae (positive sinkage upwards and positive trim bow-up):

$$\sigma = Z/\rho g A_{w} \tag{15}$$

$$\tau = M/\rho g I_{yy} \tag{16}$$

where  $A_w$  denotes the water plane area and  $I_w$  represents the longitudinal moment of inertia of the water plane area about the center of floatation. The vertical displacement of the fore and aft perpendiculars zFP and zAP can be computed by:

$$zFP + zAP = 2\sigma \tag{17}$$

$$zFP - zAP = L_{pp}\tau \tag{18}$$

Fig. 9 reports the vertical displacement of the fore and aft perpendiculars. Reasonable correspondence between the computational and experimental data can be noted.

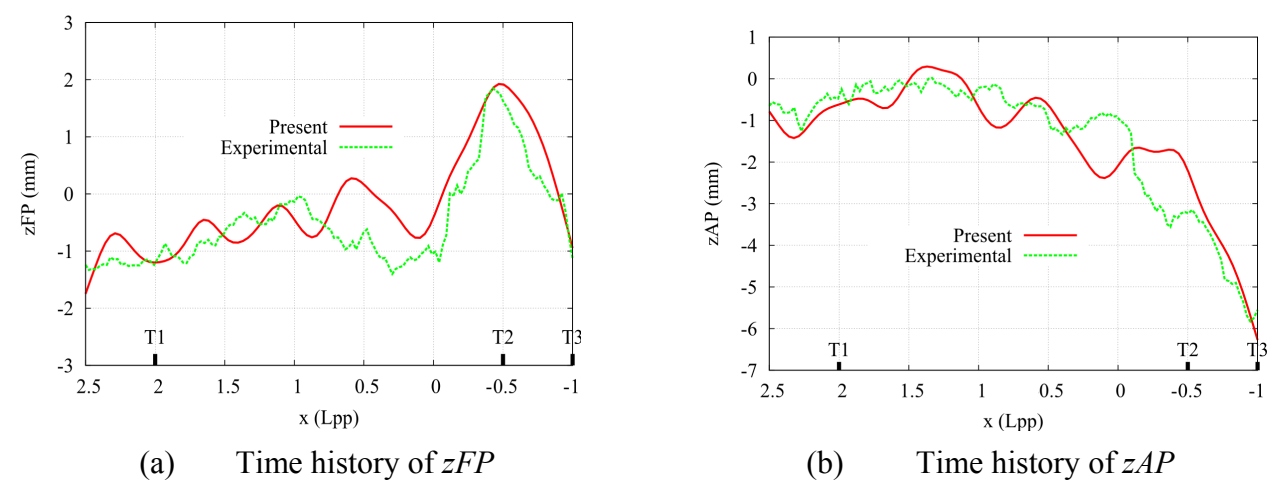


Fig. 9 Time history of zFP and zAP

Three stages in the development of zFP are shown in Fig. 9a. Firstly, negatively zFP, which is caused by the shallow water effect, with insignificant oscillation is noticed when the ship maneuvers in the approach channel. This is caused by the low speed. Then, an initial rising of the bow, which might be caused by the accumulation of water in front of the ship, can be noticed when the ship entering the lock. Thirdly, once more than half of the vessel is inside of the lock, the sinkage oscillation of zFP decreased. This is induced by the evacuation of the water in the lock. When the ship has entered the lock, the sinkage of the bow disappears. Fig. 9b manifest that the vertical displacement of the aft perpendiculars zAP is increasing as the ship entering the lock. This might be caused by the continuous declination of the surface pressure of the aft-body of the ship.

The increasing of the relative speed between ship and return flow, as well as the sinkage of water level around the stern induce the decrease of the surface pressure of the aft-body of the ship, so that the aft perpendiculars moves vertically downward.

The results of hydrodynamic forces and moments, as well as the vertical displacements show good agreement with the experimental data, which demonstrates that FDM method can accurately simulate the viscous flow around the ship with relatively small amounts grids. The results also indicate that the currently used numerical methods are suitable for studying the viscous flow around the ship during the entering manoeuvre into a lock with different eccentricity, which is presented in the next section.

# **Results of Systematic Computations**

The effect of eccentricity on the characteristic of the viscous flow around the ship, during the entering manoeuvre of a ship into a lock is significant. In order to give a clear insight into the ship behavior when entry the lock with different eccentricity, case A1 and case A2 were carried out. The details of the test conditions for the systematic study was given in table 2.

# Hydrodynamic Forces

Fig. 10 presents the hydrodynamic forces and moment of the 12000TEU ship model when entry into the lock with different lateral position. All the results show that the eccentricity increases do not alter the general pattern of the forces and moment, but just cause higher extreme values. The results declare that more pronounced prevention of water in the lock from evacuate out can be noticed with increasing eccentricity. So, more water in the lock might be accumulated in the lock, which causes higher velocities of the return flow. Accordingly, the longitudinal force *X* increases. Furthermore, the flow around the ship will be more asymmetric with higher eccentricity. As the ships are allowed with very small side margins in the lock, higher eccentricity represents higher risk of collision of ship and side walls. So, protection measures, such as fenders, are suggested.

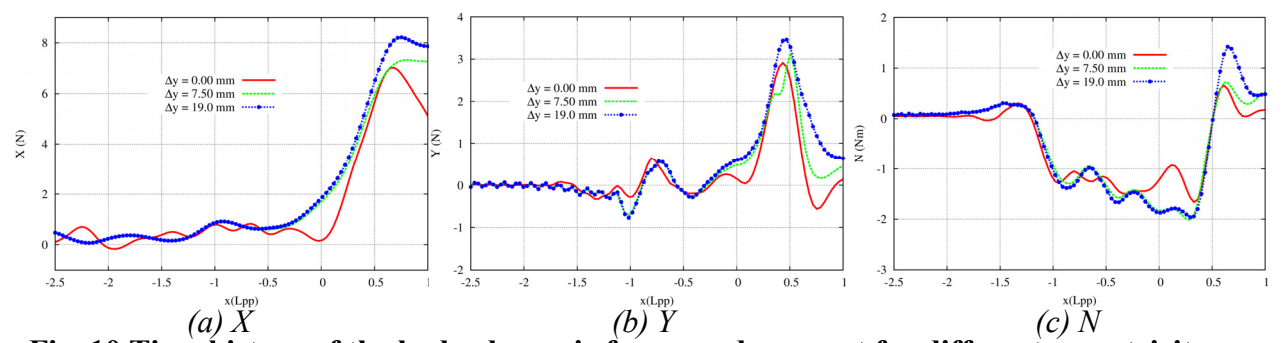


Fig. 10 Time history of the hydrodynamic forces and moment for different eccentricity cases

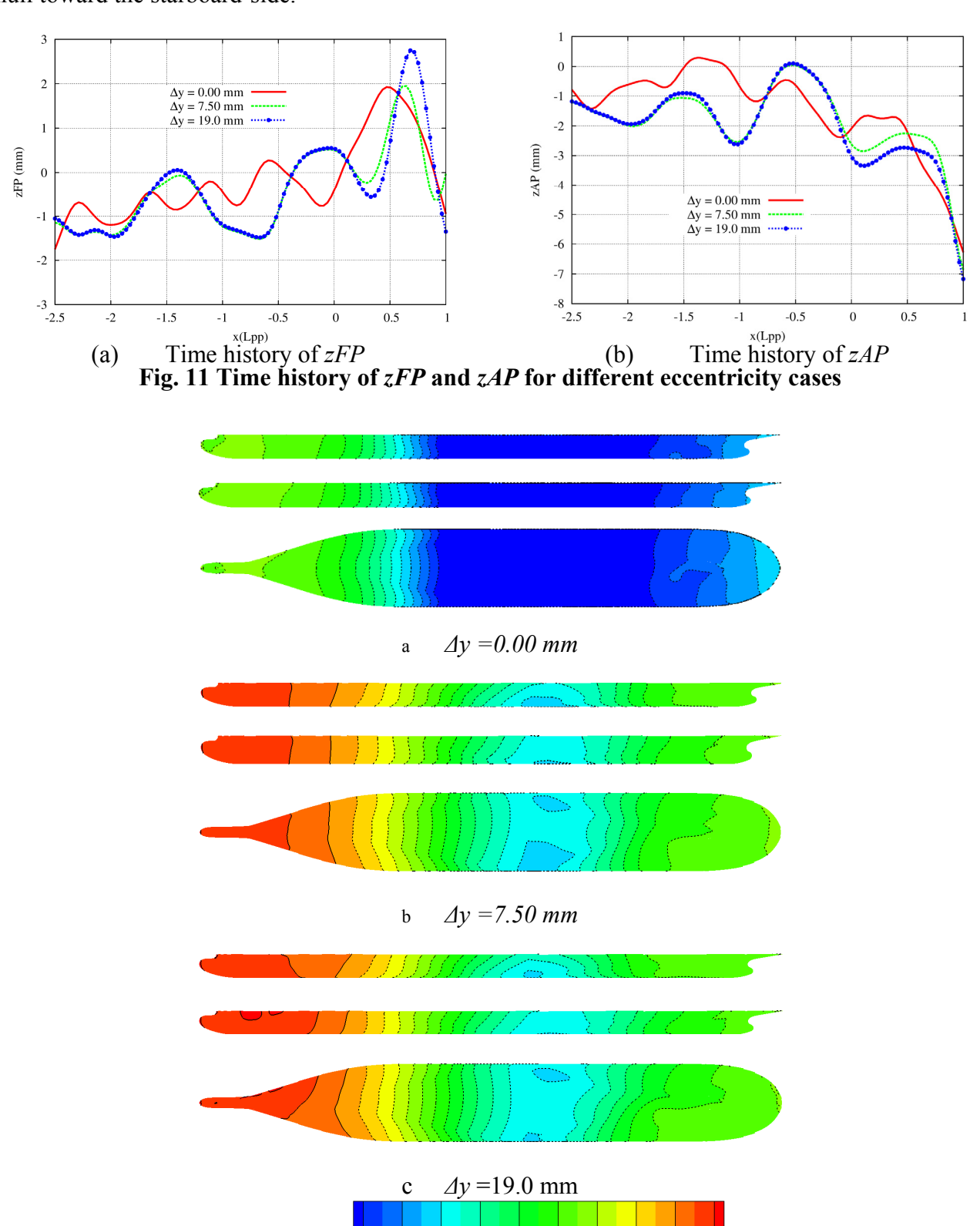
### Vertical Displacements

The vertical displacement of the fore and aft perpendiculars zFP and zAP for different lateral position are computed and presented in Fig. 11. Both of zFP and zAP increase with increasing eccentricity. This causes higher risk of bottom touch. Due to the high blockage of the lock, especially the shallow water effect, the increase of the risk of bottom touch are noteworthy. According to the results, moving along the lock's centerline is the safest way when maneuvering into a lock.

#### *Surface pressure distribution*

Fig. 12 presents the computed results of the surface pressure at time T3 for different eccentricity cases. Firstly, higher surface pressure around fore-body than that around aft-body is shown in all cases. This is causes by the higher water level elevation in the vicinity of the fore-body. Secondly, the results also manifest that the surface pressure, as well as the asymmetry of the surface pressure increases with increasing eccentricity. The difference of surface pressure between port and starboard sides is mainly concentrated in the aft-body of the hull and the surface pressure on the

starboard side is larger than that on the port side. As a result, a negative yaw moment will turn the hull toward the starboard-side.



Pr(Pa): -80 -70 -60 -50 -40 -30 -20 -10 0 10
Fig. 12 Pressure (port side view, starboard side view and top view) against different ship speed at time T3

#### **Conclusions**

Effects of eccentricity on the hydrodynamics of a ship while entering a lock were investigated and reported in this paper. The capability of the present method for the prediction of the viscous flow around the ship model when entering the lock is confirmed by the good agreement of the predicted results with the corresponding experimental data. The hydrodynamic forces, vertical displacements were presented and discussed. A significant effect of high blockage on the hydrodynamic forces and moment, as well as ship sinkage was noticed. Furthermore, FDM method is especially suitable for solving low speed headache with remarkable free surface effects.

A systematic investigations were then made to examine the effects of the eccentricity on the hydrodynamics on the ship when it enter a lock. According to the results, several interesting observations can be made:

- 1. Hydrodynamic forces moment, as well as the sinkage of the ship are sensitive to the eccentricity.
- 2. Hydrodynamic forces and moment, as well as the sinkage of the ship, increase with increasing eccentricity. This causes the increases of the difficulty to manoeuvre a ship into a lock, safely.
- 3. When the eccentricity increases, an increase of the risk of side collision is observed.
- 4. When entering a lock, moving along the lock's centerline and protection measures is suggested.

#### Acknowledgement

This work is supported by National Natural Science Foundation of China (Grant Nos. 51379125, 51490675, 11432009, 51411130131, 11272120), The National Key Basic Research Development Plan (973 Plan) Project of China (Grant No. 2013CB036103), High Technology of Marine Research Project of The Ministry of Industry and Information Technology of China, Chang Jiang Scholars Program(Grant No. T2014099) and the Program for Professor of Special Appointment (Eastern Scholar) at Shanghai Institutions of Higher Learning(Grant No. 2013022), to which the authors are most grateful.

#### References

Chen, X. N. (2010) From water entry to lock entry, Journal of Hydrodynamics, Ser. B, 22(5), 885-892.

Delefortrie, G., Willems, M., et al. (2008) Tank test of vessel entry and exit for third set of Panama locks, *In Proceedings of the International Navigation Seminar following PIANC AGA*, 517-523.

Delefortrie, G., Willems, M., et al. (2009) Behavior of post panamax vessels in the Third Set of Panama locks, In International Conference on Marine Simulation and Ship Maneuverability (MARSIM'09).

Meng, Q. J., & Wan, D. C. (2014) Numerical Simulations of Ship Motions in Confined Water by Overset Grids Method, In The Twenty-fourth International Ocean and Polar Engineering Conference.

Menter, F. R. (1994) Two-equation eddy-viscosity turbulence models for engineering applications, *AIAA journal*, **32(8)**, 1598-1605.

Osher, S., & Sethian, J. A. (1988) Fronts propagating with curvature-dependent speed: algorithms based on Hamilton-Jacobi formulations, *Journal of computational physics*, **79(1)**, 12-49.

Richter, J., Verwilligen, J., et al. (2012) Analysis of full ship types in high-blockage lock configurations, *In MARSIM* 2012, 1-9.

Sethian, J. A., & Smereka, P. (2003) Level set methods for fluid interfaces. *Annual Review of Fluid Mechanics*, **35(1)**, 341-372.

Sussman M, Smereka P, Osher SJ. (1994) A level set approach to computing solutions to incompressible two-phase flow, *Journal of Computational physics*, **114(1)**, 146-159.

Vantorre, M., Delefortrie, G., Mostaert, F. (2012) Behaviour of ships approaching and leaving locks: Open model test data for validation purposes. Version 2\_1, *WL Rapporten*, **WL2012R815\_08e**, Flanders Hydraulics Research and Ghent University - Division of Maritime Technology: Antwerp, Belgium.

Vergote, T. (2012) Hydrodynamics of a ship while entering a lock. Eng. thesis, Ghent Univ., Ghent, Belgium.

Vrijburcht, A. (1988) Calculations of wave height and ship speed when entering a lock, *Delft Hydraulics Publication* **391**, 1-17.

Wang, H. Z., & Zou, Z. J. (2014) Numerical study on hydrodynamic interaction between a berthed ship and a ship passing through a lock, *Ocean Engineering*, **88**, 409-425.